

**Paper No.**  
16789



## **Prediction of Top of Line Corrosion Risk due to Damages in External Pipeline Insulation**

Marc Singer

Institute for Corrosion and Multiphase Technology, Ohio University  
342 West State Street, Athens OH 45701, USA  
[singer@ohio.edu](mailto:singer@ohio.edu)

Nick Bardsley, Julie Morgan, Stuart Kegg, Adam Darwin  
Woodside Energy Ltd

Peter Cossins, Anthony Kwong, Jason Biddlecombe, Jo Yetman, Joe Bullen  
Frazer-Nash Consultancy Ltd

### **ABSTRACT**

This paper presents the methodology adopted to evaluate the effect of external insulation damage on TLC within carbon steel flowlines. A field development, consisting of subsea wells in 830 m water depth, transports wet gas via two 20" diameter production flowlines. The wet gas contains about 1.5 to 2 mol% CO<sub>2</sub>. The pipeline system is largely carbon steel with only short lengths made of CRA piping. Lean MEG mixed with corrosion inhibitor is injected at the wellheads for hydrate inhibition. A subsea remotely operated vehicle inspection of the deep water 20" spools revealed insulation damage and bulging. These damages could act as cold spots and lead to enhanced water condensation and TLC on the internal wall of the flowlines. In order to assess the severity of the impact of the damages, a thermal Finite Element Analysis step was undertaken to determine the condensation rates on the inside of the lines. The corresponding TLC rates were then calculated using mechanistic corrosion prediction software considering multiple production conditions. The corrosion assessment helped identify which insulation damages required remedial actions. The TLC rates calculated were later verified by internal pipeline pigging inspection.

Keywords: Insulation, Top of Line Corrosion, Corrosion management, Thermal mapping

### **INTRODUCTION**

A visual inspection of a subsea field development, transporting wet gas, containing approximately 1.5 to 2 mol% of CO<sub>2</sub> to shore, was conducted via ROV (remotely operated vehicle). The pipeline system is largely carbon steel with only short lengths of CRA (corrosion resistant alloy) piping from the wellhead to the production/pigging manifold. Downstream of the pigging manifold the system has 20" carbon steel spools leading to the FTA (flowline termination assembly) and then 20" carbon steel flowlines to the riser platform. Lean MEG (monoethylene glycol) is injected at the wellheads for hydrate inhibition and corrosion inhibitor is mixed with the lean MEG to mitigate

bottom of line corrosion within the pipeline system. The spools and flowline are insulated to control water condensation rates such that the resulting TLC (top of line corrosion) rate can be within the limits of allowed corrosion.

The inspection of the 20" spool piece between the pigging manifold and the FTA revealed that some of the pipeline insulation had been damaged and became partially or fully detached. Bulging was also observed on some locations. The damage resulted from pipeline walking, causing spool deflection and subsequent interaction between the spool insulation and supporting mud mat. These insulation damages could act as cold spots (locations where the internal pipe wall temperature is lower temperature than adjacent areas of pipe where external insulation is intact) and lead to enhanced WCR (water condensation rate) and TLC rates on the internal wall of the flowlines.

## OBJECTIVES

The primary objective of this work was to evaluate the effect of external insulation damages on TLC within the flowline spools. The results would provide understanding of the risk and predicted rates of TLC and inform the forward plan for pipeline system integrity management. Specific flow rate cases were selected, representing historic flow conditions along the flowline spools.

This work was performed using the BLC/TLC prediction software MULTICORP/TOPCORP<sup>1</sup> (identified as Corrosion Software in the rest of the paper) developed by the Institute for Corrosion and Multiphase Technology at Ohio University [1-5]. Corrosion Software is mechanistic corrosion prediction software equipped with simplified (i.e. steady state) flow assurance capabilities.

In most cases, WCR inputs were obtained through a thorough thermal analysis performed by Frazer-Nash Consultancy using OLGA<sup>1</sup> (identified as Flow Assurance Software in the rest of the paper). These WCR inputs are used directly to predict TLC rates. The simulation conditions are detailed in the methodology section and the presentation of the results.

## SYSTEM DESCRIPTION

### Flowline characteristics

The two 20" ID flowlines are about 170 m long and are considered to be horizontal. Their characteristics are shown in Table 1.

**Table 1**  
**Pipeline thermal insulation characteristics**

<b>20 " Flowline Summary</b>	
U Value (W/m <sup>2</sup> /K)	7.4
Pipe Roughness (mm)	0.03
Pipe ID (m)	0.457
Wall Thickness (m)	0.0318
Environment	Sea
Sea temperature (°C)	5
Sea water wind velocity (m/s)	0.1
<b>Thermal Insulation</b>	
Conductivity (W/m/K)	0.167
Thickness (mm)	23

---

<sup>1</sup> : Trade name

### Fluid composition and formation water properties

One CO<sub>2</sub> level was considered: 2 mol%. No H<sub>2</sub>S has been detected in these lines. The undissociated VFA (volatile fatty acid) content is set at 40 ppm, although sensitivity cases without any VFA were also considered.

### Fluid flow rates

Table 2 presents the overall operating envelope that was used for the study. More cases, representing historic, current and future production conditions were considered but are not shown in this publication.

**Table 2**  
**Flow cases operating envelope**

Flowlines & Case No.	Operating conditions	Fluid Composition [wt.%]				Liquid Mass Flow Rate [kg/s]	Liquid Density [kg/m <sup>3</sup> ]	Gas Mass Flow Rate [kg/s]	Gas Density [kg/m <sup>3</sup> ]
		Production Fluid (liq)	MEG (liq)	Water (liq)	Gas Mixture				
A-1	Nominal	4.98	1.03	0	93.99	6.93	841.57	108.33	101.21

### Insulation damage cases

Several locations of insulation damage were detected on flowline A and B. The following cases were modelled to investigate their effect on WCR and TLC rates.

Case 1 represents intact external insulation.

Case 2 represents pipe with no insulation.

Case 3: 90° insulation damage (Table 3)

- Insulation disbondment between 3 and 6 o'clock.
- Seawater could be present as a film directly around the pipe in a stagnant state as that full adhesion of the remaining insulation cannot be guaranteed.

**Table 3**  
**Detailed description of anomaly case 3**

	<p>Summary:</p> <ul style="list-style-type: none"> <li>• Insulation was found to be damaged/dislodged on eastern side, 350mm wide x approx. 250 mm long. End not seen at 6 O'clock position.</li> <li>• Heat diffraction was obvious at upper edges of perforation/tear.</li> <li>• Small section of spool sighted within the dislodged insulation appeared to have paint coating intact.</li> <li>• The damage only evident on the eastern face.</li> </ul>
-------------------------------------------------------------------------------------	--------------------------------------------------------------------------------------------------------------------------------------------------------------------------------------------------------------------------------------------------------------------------------------------------------------------------------------------------------------------------------------------------------------------------------------------------------------

Case 4: 30° insulation damage (Table 4)

- Insulation disbondment between 5 and 6 o'clock.
- Seawater could be present as a film directly around the pipe in a stagnant state as we full adhesion of the remaining insulation cannot be guaranteed.

**Table 4**  
**Detailed description of anomaly case 4**

	<p>Summary:</p> <ul style="list-style-type: none"> <li>• The insulation was found dislodged on the eastern side, approximately 200 mm long and 100mm wide.</li> <li>• Heat diffraction for the damage was noted.</li> <li>• Small section of spool sighted within the dislodged insulation appeared to have paint coating intact.</li> <li>• The insulation damage was only evident on the eastern side.</li> </ul>
--	---------------------------------------------------------------------------------------------------------------------------------------------------------------------------------------------------------------------------------------------------------------------------------------------------------------------------------------------------------------------------------------------------------------------

## THERMAL ANALYSIS

### Methodology

To determine the 3D temperature profile within the line, a thermal FEA (finite element analysis) model was set up in Abaqus 2017™, taking into account the line and insulation geometry, thermal properties of the material, operating conditions and internal liquid level. Previous multi-phase CFD (computational fluid dynamics) analysis had shown that within the 20" line flow stratification into separate condensate and gas phases was likely at all operating conditions, with a liquid depth of approximately 5cm for the cases under consideration here, as shown in Figure 1 for typical Flowline A results.

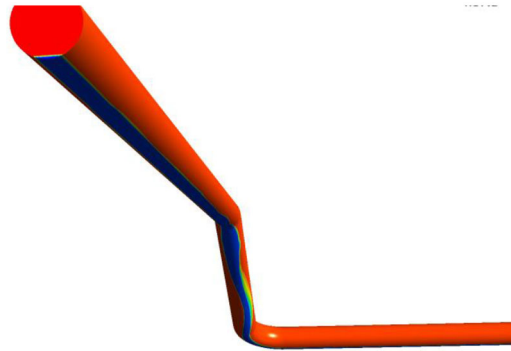


**Figure 1: CFD predicted gas volume fraction at exit to the flowline termination assemblies. Blue indicates the presence of a liquid phase. Red indicates the gas phase, where water condensation and TLC can occur. Intermediate colors indicate regions that vary between liquid and gas phases.**

### Analysis Summary

The analysis method can be summarized as follows:

- A 3D model was created and meshed with quadratic elements, including the steel pipe wall and (where necessary) the external insulation, including any damaged regions.
- Thermal properties were assigned to all components as follows:
  - Source and sink temperatures were set for the internal and external fluids;
  - Thermal conductivity values were provided for the steel and insulation materials.
  - All internal and external surfaces were assigned a heat transfer coefficient, to determine the transfer of heat from the fluid into the surface (internal) or vice versa for external surfaces;

These properties are sufficient to determine the heat fluxes and material temperatures throughout the system

- The thermal FEA solver then iterates to determine the 3D heat fluxes and temperatures for every cell within the model, until a steady state equilibrium condition is reached.

- Once converged, the temperature differential between the gas temperature and the local wall temperature was used to calculate the water condensation rate at each point on the gas-washed inner surface of the line.

### Geometries Assessed

Four separate three-dimensional run geometries were considered:

- Case 1: Nominal case with 23mm of complete insulation around the entire circumference;
- Case 2: Uninsulated case, all insulation removed;
- Case 3: Damaged conditions, 90° of insulation loss from the three o'clock to six o'clock positions over a 350mm length of line;
- Case 4: Damaged conditions, 30° of insulation loss from the five o'clock to six o'clock positions over a 300mm length of line.

In all cases, the computational domain was large enough to encompass the entire region thermally affected by the insulation damage, ensuring the model was independent of the pipe end conditions.

### Thermal Properties

For all four cases the internal gas temperatures was set to 58.9°C, and the sea water temperature was set to 5.4°C.

The thermal conductivity of the API 5L X65 steel line was set to 45 W/(m·K). The thermal conductivity of the insulation was taken as 0.167 W/(m·K). Based on information related to the outside environment [6], a typical seabed thermal conductivity of 1.1 W/(m·K) was assumed when calculating the heat transfer coefficient into the seabed.

All external and internal surfaces of the thermal FEA model had heat transfer coefficients applied, as shown below in Figure 2 for Run 3 (90° damage case, note that the figure does not show actual model mesh, which is significantly finer).

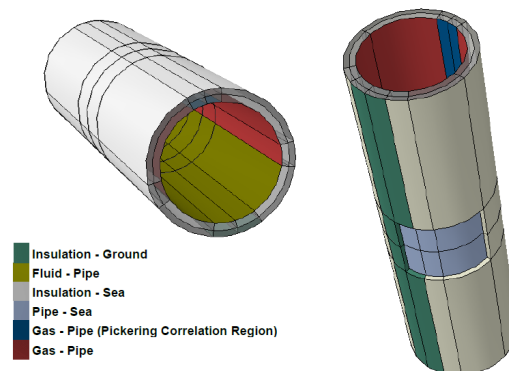


**Figure 2: Heat transfer zones applied to the thermal model**

Gas to pipe internal walls: The average thermal resistance for the overall system, combined with the gas and internal wall temperatures (all from Flow Assurance Software), allowed the heat transfer coefficient (HTC) from the gas into the wall to be calculated as 1,882 W/(m<sup>2</sup>·K).

Liquid to pipe internal walls: The HTC from the liquid into the internal wall of the line was determined from standard empirical relationships for turbulent flows in pipes and was calculated to be 909 W/(m<sup>2</sup>·K).

External wall to seawater: Using the overall thermal resistance provided from the Flow Assurance Software together with material thermal conductivities, the HTC from the external wall into the seawater was calculated by considering the thermal resistances from each of the separate components. The resultant value of  $509 \text{ W}/(\text{m}^2\cdot\text{K})$  was compared against typical HTCs expected for a cylinder in cross flow (using a current velocity of  $0.2\text{m/s}$  and typical empirical correlations [7]) and found to be in good agreement. This was applied over the region  $\pm 20^\circ$  either side of the bottom of the line.

External wall to seabed: Based on soil models for submerged lines, a conduction region was assumed to exist around the line. The outer radius was taken as three times the outer radius of the line [8], and this was combined with the seabed thermal conductivity [9] to infer an HTC of approximately  $4\text{W}/\text{m}^2\cdot\text{K}$  from the external wall into the seabed. Given the insulating effect of the seabed, the sensitivity of the results to the exact value of this HTC is small.

### Model verification and sensitivity assessment

In order to check that the calculated HTCs were valid, cases 1 and 2 (with undamaged insulation and with no insulation respectively) were compared against the one-dimensional Flow Assurance Software results for the same operating condition. They showed very good agreement, with a maximum heat flux error of less than 1.7%.

In order to understand the sensitivity of the results for contact with the seabed, a study was undertaken in which the overall seabed contact angle was reduced from  $40^\circ$  to  $20^\circ$  about the bottom of the line. The resulting impact on the wall temperatures at the top of the liquid level was negligible, changing by approximately  $0.01^\circ\text{C}$ . All models were therefore run with a constant contact angle of  $40^\circ$ .

### Condensation Calculation

Condensation rate calculations were undertaken based on considerations of the balance between gravity and drag forces on the forming droplets. This led to two different scenarios, as discussed in [4]:

- a) At gas flow velocities above  $\sim 3\text{m/s}$ , the drag force on the droplets is likely to make them unstable and will tend to drive them along the length of the pipe. As such the condensation rate is dominated by filmwise condensation (i.e. a thin liquid film is always present on the steel surface and condensation occurs at the liquid/vapor interface). The spatially averaged condensation rate in this scenario is determined based on the water content of saturated gas (as used in Flow Assurance Software) and is assigned for all gas-washed surfaces.
- b) At lower flow velocities the drag force from the gas is significantly reduced, and calculations have shown that droplets within  $\pm 13.4^\circ$  of the top of the line are the most stable. This region is therefore vulnerable to dropwise condensation (condensation occurs at the solid/vapor interface by forming droplets). Dropwise condensation can generate heat transfer rates ten times higher than for filmwise conditions in similar conditions. An in-house WCR correlation, identified as the Pickering condensation correlation, has been applied within this top region for the second scenario.

## **Results**

For each of the four cases considered, plots of steady state nodal temperature response are developed. The combined Flow Assurance Software correlation condensation rate is shown together with the Pickering correlation rate applied at the top  $22.8$  degrees of the inner diameter. In addition, for cases 3 and 4, the circumferential steady state nodal temperature response is plotted at the pipes axial mid-span anti-clockwise from the TDC (top dead center). It is also plotted

at the internal diameter along the axial length of the pipe at various angular positions. The series for case 1 to 4 are shown in Figure 3 to Figure 10.

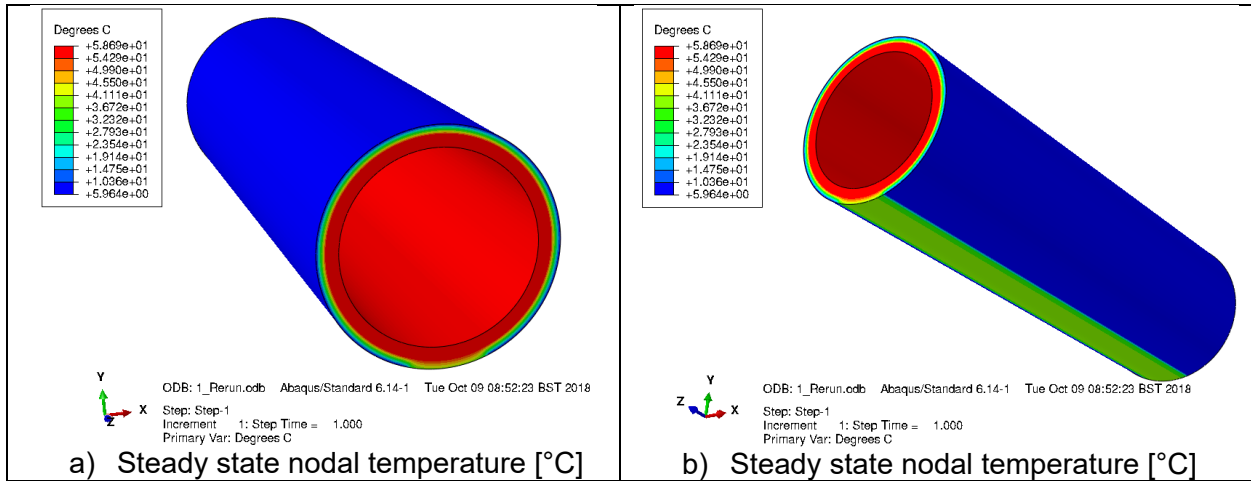


Figure 3: Case 1 – Full insulation – Temperature profiles

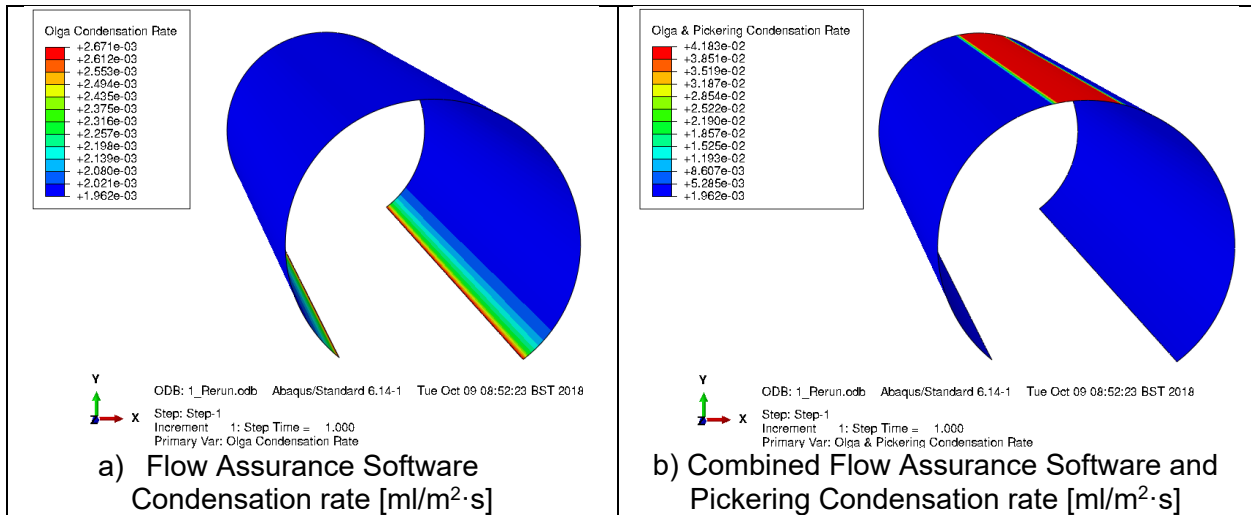


Figure 4: Case 1 – Full insulation – Profiles of WCR

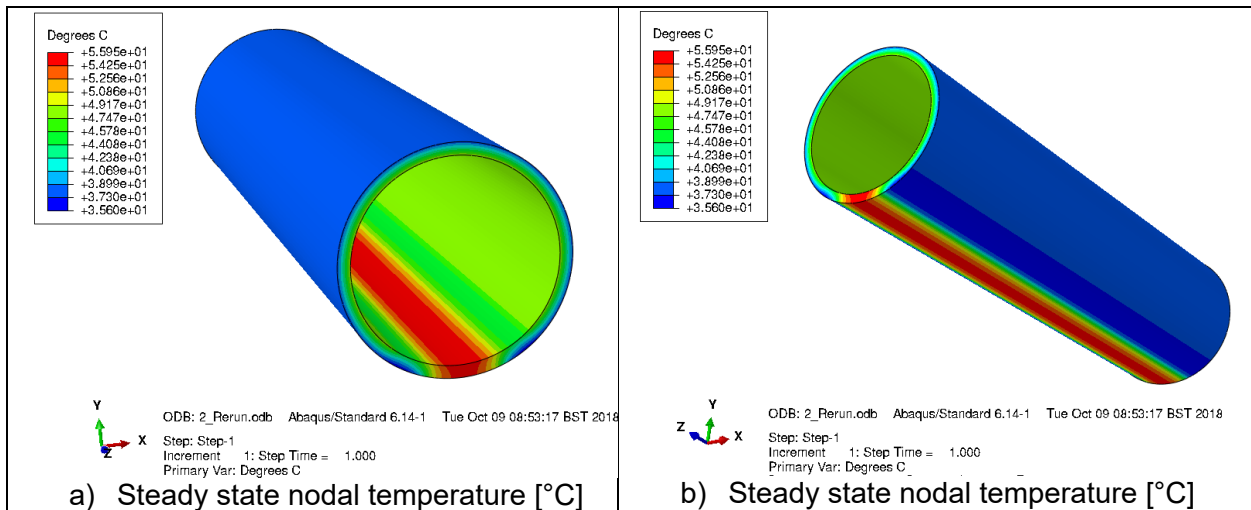
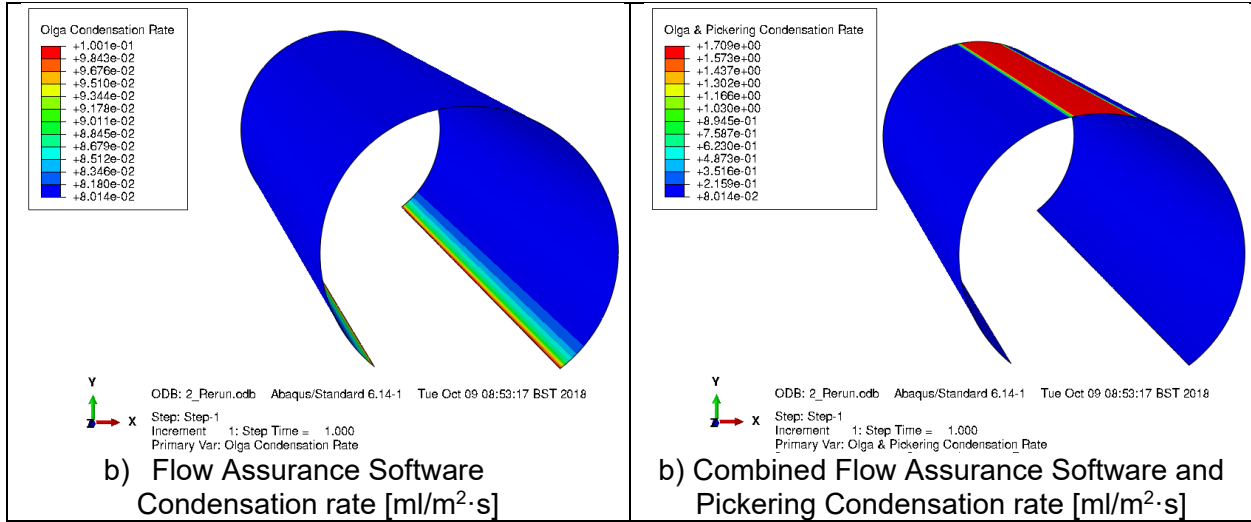
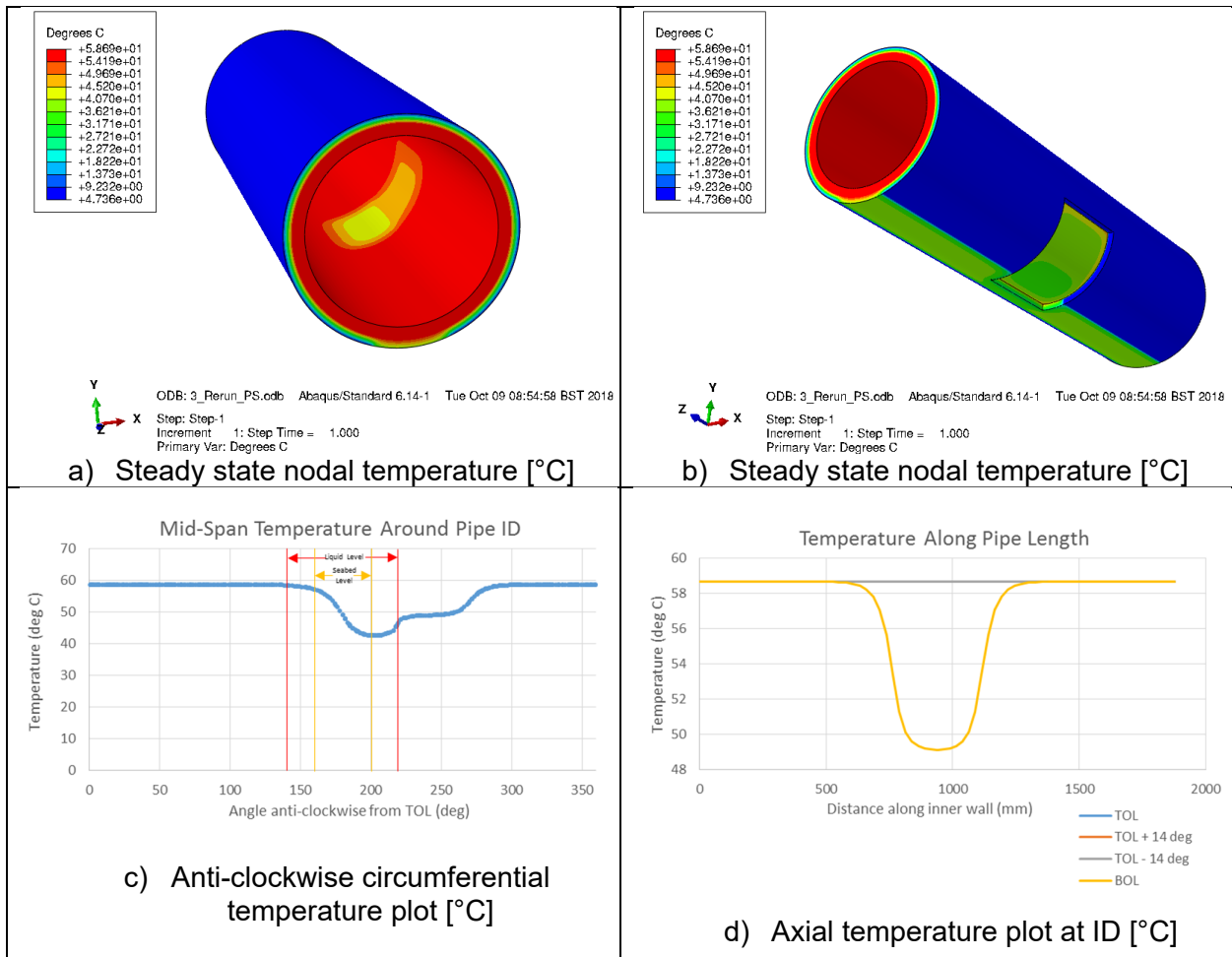


Figure 5: Case 2 – No insulation – Temperature profiles



**Figure 6: Case 2 – No insulation – Profiles of WCR**



**Figure 7: Case 3 – 90 degree, 350 mm damage, 5cm liquid level – Temperature profiles**

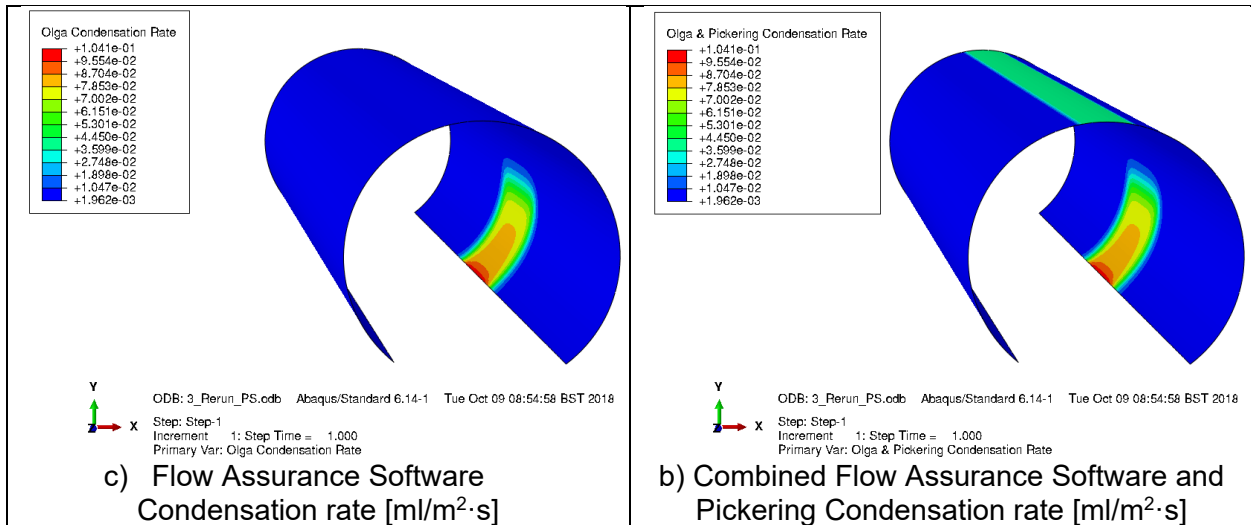


**Figure 8: Case 3 – 90 degree, 350 mm damage, 5cm liquid level – Profiles of WCR**

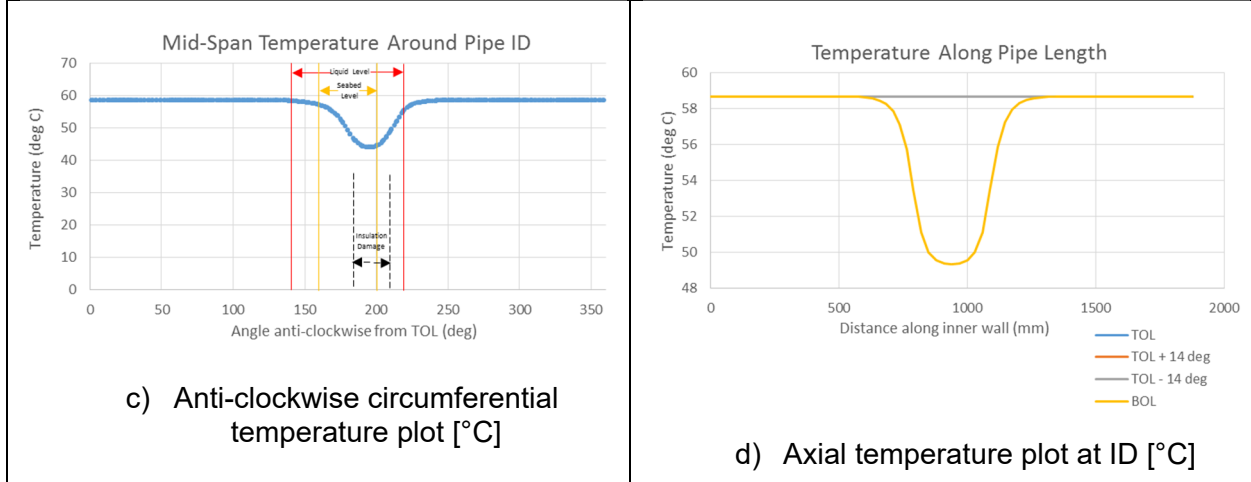
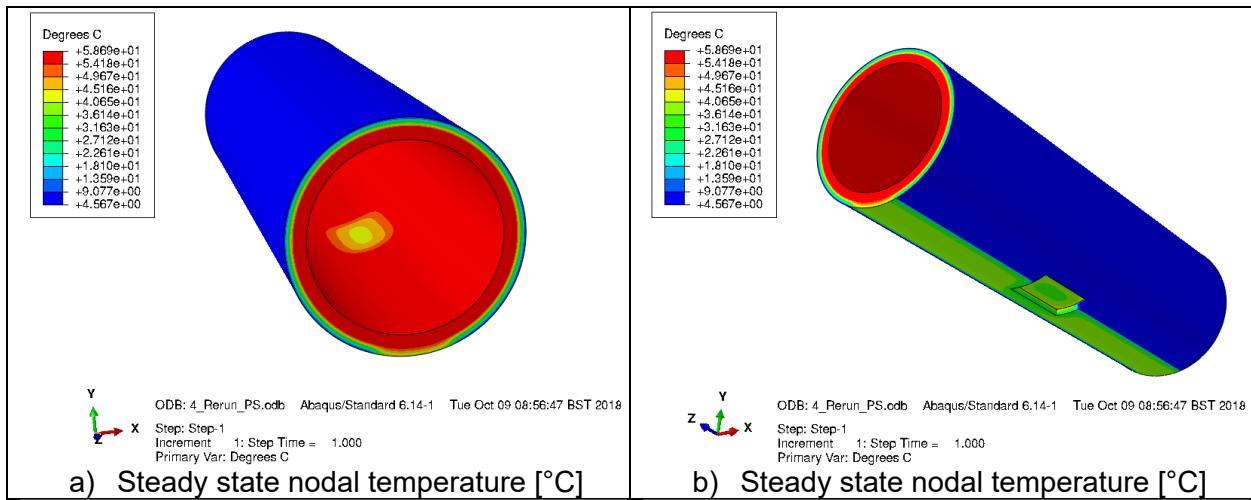


**Figure 9: Case 4 - 30 degree, 350 mm damage, 5cm liquid level – Temperature profiles**

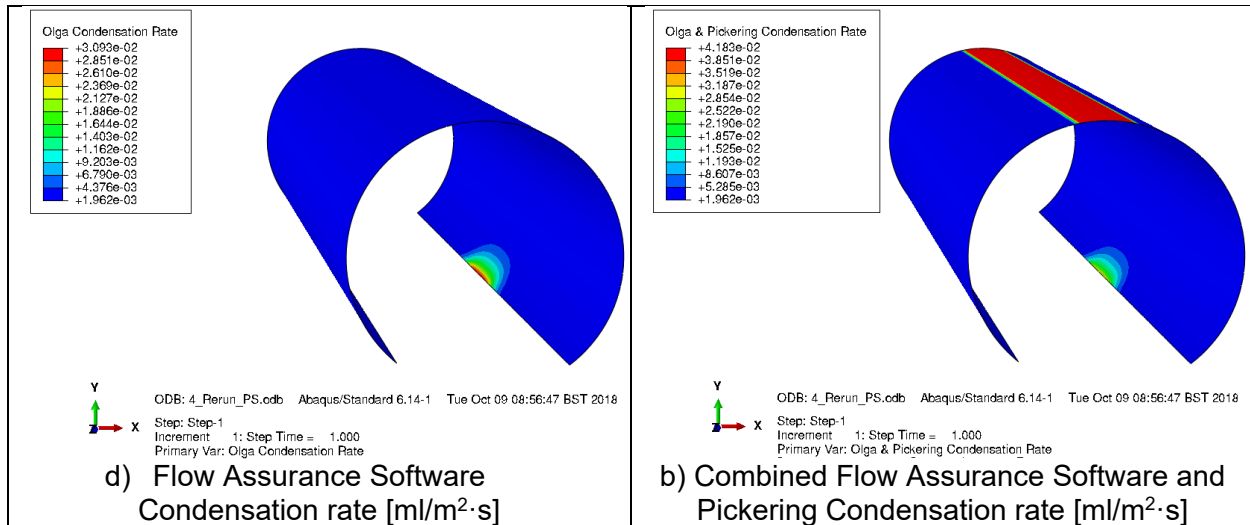


**Figure 10: Case 4 – 90 degree , 350 mm damage, 5cm liquid level – Profiles of WCR**

## CORROSION ASSESSMENT

### Methodology

The corrosion prediction work was performed using Corrosion Software and involved point modeling, considering that WCR input from Flow Assurance Software are used to predict TLC at discrete locations along the flowline.

As mentioned above, the WCRs obtained from the thermal analyses were used as input parameters, instead of using Corrosion Software to directly calculate WCR data. Since WCR is not a “true” input in Corrosion Software, the thermal insulation thickness was adjusted to match the data provided. Typically, only slight variations in insulation thickness were required.

While the WCR at the anomaly location was calculated using Computational Fluid Dynamics software in conjunction to flow assurance modeling, the WCR at the top of the line was determined using an in-house correlation labelled Pickering Correlation. This correlation is based on a fitting exercise over WCR data generated with Corrosion Software. Although a fitting equation will have limited validity compared to the original Corrosion Software condensation module, it can be used with confidence as long as the range of conditions is within the range for which the correlation was developed. The Pickering correlation was developed with data obtained in the presence of MEG, it should not be expected that its domain of validity extends to environments without MEG.

Steady state point TLC simulations were then performed along the circumference of the pipeline corresponding to the locations of the insulation damage (if any). TLC rates were determined considering 0 and 40 ppm VFA, and one CO<sub>2</sub> content: 2 mol%.

### Corrosion simulation results

The TLC rate predictions for case 1 through 4 are displayed in Figure 11 through Figure 14.

Comments are directly added on each graph to aid the understanding of the data:

- The greyed out area in the middle of each plot corresponds to the location of the liquid phase, where no TLC calculation can be performed.
- WCR predictions are shown in light blue, a filmwise condensation model, developed by the Flow Assurance Model, was used to generate the WCR plot on the sides of the

pipeline, while a dropwise condensation model, identified as the Pickering correlation, was used to calculate the WCR at locations within  $\pm 13.4^\circ$  of the top of the line.

- TLC rates were calculated at several points along the circumference of the pipe, with a focus on the insulation damage location (if any) and on the top of the line. In each case the TLC rate is directly correlated to the WCR, i.e. TLC rates corresponding to the same WCR value holds identical values since the rest of the input conditions remain unchanged. Consequently, although the TLC rates were not calculated for every point, the trend along the circumference of the pipe can be easily deduced.
- Black dots correspond to conditions considering 0 ppm of VFA while yellow dots correspond to conditions with 40 ppm VFA.
- TLC rates corresponding to WCR below 0.01 mL/m<sup>2</sup>/s are assumed to be below 0.05 mm/year, which corresponds to the low limit of Corrosion Software prediction.
- In case 4, the internal wall cold spot extended beyond the area of external insulation damage due to the pipe steel's high thermal conductivity, resulting in an increased area affected by TLC.

Finally, the TLC rates predicted by the Corrosion Software are meant to be conservative. For comparison purposes, any rate below 0.1 mm/year should be considered as low TLC risk [5].

### Case 1 – Full Insulation

#### Mid-Span Condensation and TLC Rate Around Pipe ID

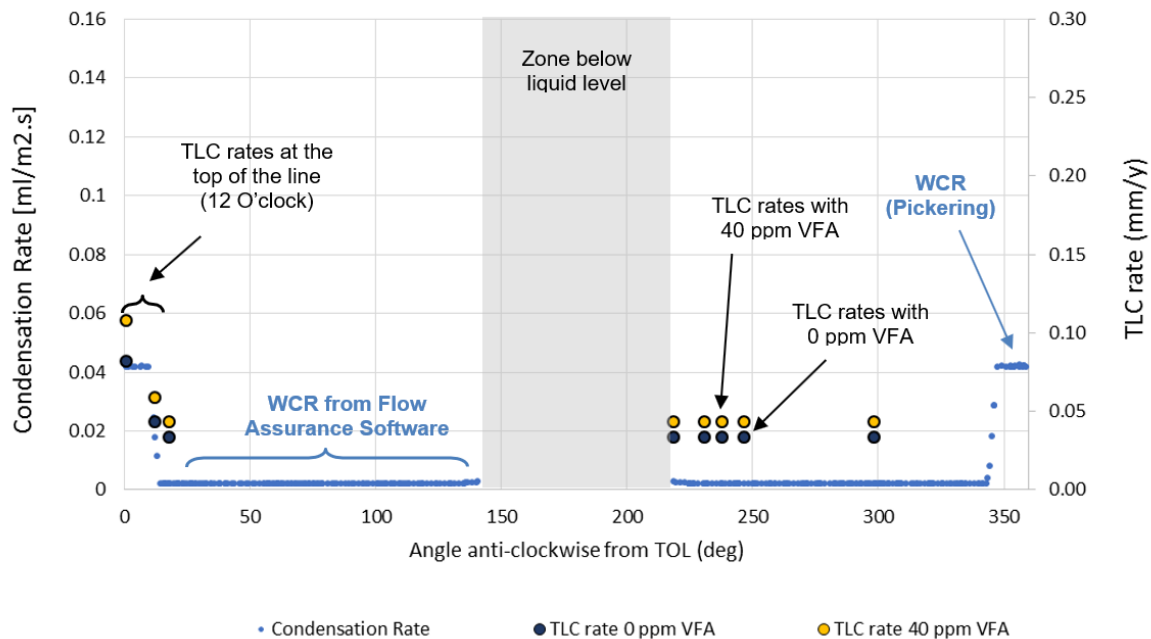


**Figure 11: Case 1 - Profile of WCR and TLC rate  
2 mol% CO<sub>2</sub> – 0 and 40ppm VFA**

Case 2 – No insulation

Mid-Span Condensation and TLC Rate Around Pipe ID

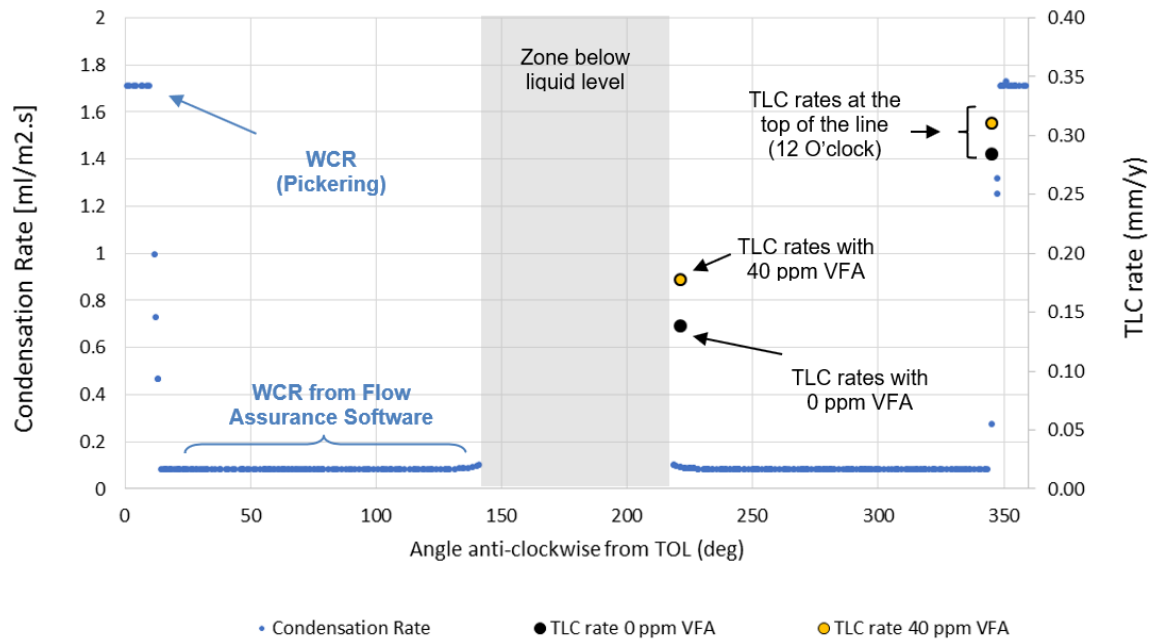


**Figure 12: Case 2 - Profile of WCR and TLC rate  
2 mol% CO<sub>2</sub> – 0 and 40ppm VFA**

Case 3 – 90° insulation damage

Mid-Span Condensation and TLC Rate Around Pipe ID

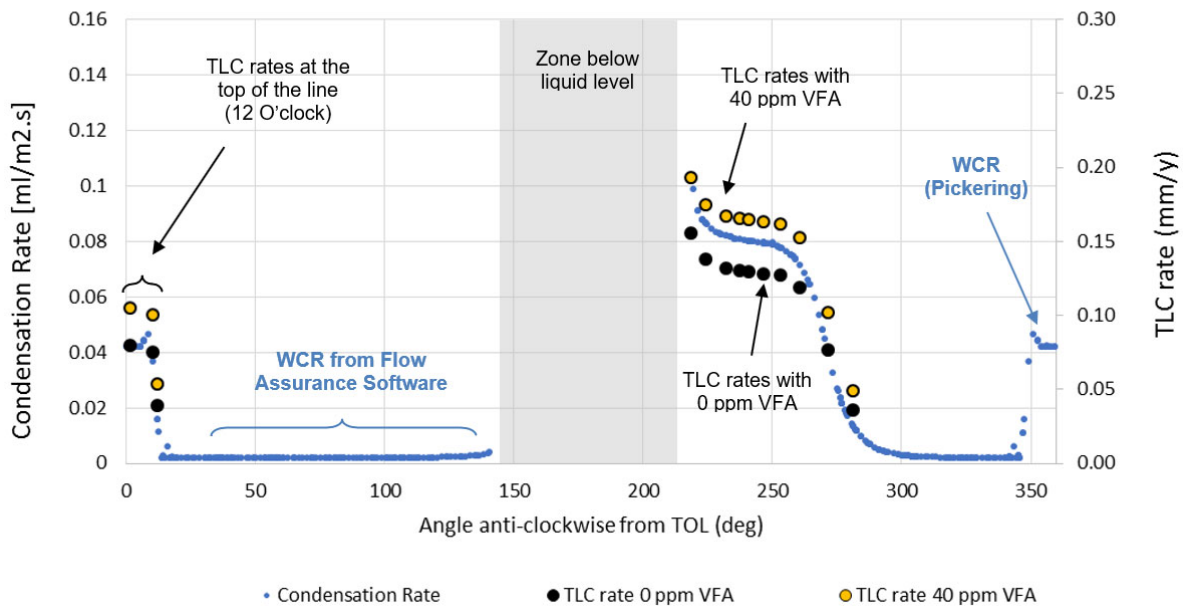


**Figure 13: Case 3 - Profile of WCR and TLC rate  
2 mol% CO<sub>2</sub> – 0 and 40ppm VFA**

## Case 4 – 30° insulation damage

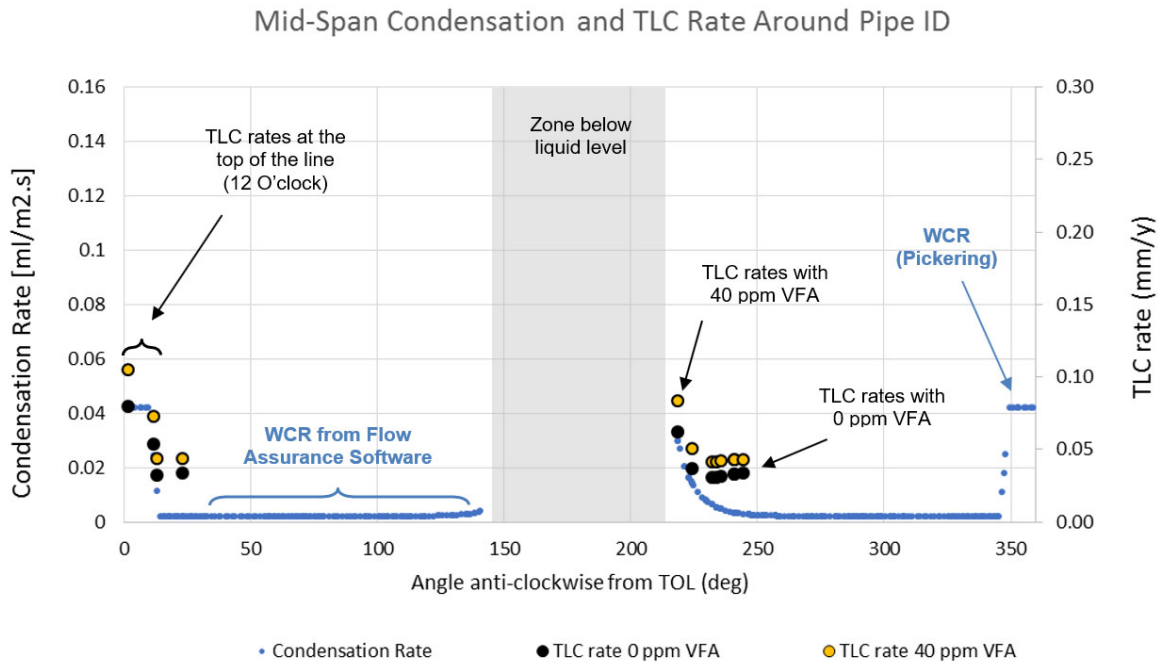


**Figure 14: Case 4 - Profile of WCR and TLC rate  
2 mol% CO<sub>2</sub> – 0 and 40ppm VFA**

## DISCUSSION

The extent of TLC predicted for case 1, considering intact insulation (Figure 11), is logically very low. TLC rates predicted by the Corrosion Software all along the circumference of the pipe were below 0.1 mm/year. The low rate of corrosion, despite a high CO<sub>2</sub> content and a high temperature, is attributed to the formation of a protective corrosion product layer made of FeCO<sub>3</sub>. The protectiveness of the layer is related, among other things, to the WCR as a low rate of water condensation will ensure the formation of a stable layer [10]. In this case, the low WCR (always below 0.05 mL/(m<sup>2</sup>.s)) was mostly due to the effectiveness of the thermal insulation and to the presence of MEG which decreased the water vapor pressure.

It is noticeable that the TLC rates are lower on the side of the pipe compared to the top. This is due to the different approaches selected to predict WCR: filmwise condensation for the side and dropwise condensation for the top of the line. As mentioned above, dropwise condensation can generate WCRs of an order of magnitude higher compared to filmwise conditions. This led to higher WCRs at the top of the line and consequently higher TLC rates. The presence of VFA also increased slightly the TLC rates as VFA co-condenses with at the top of the line and leads to a decrease in pH and a corresponding destabilization of the corrosion product layer. These comments on the effect of WCR and VFA are common for every case.

The limiting case considering no insulation (case 2) yielded logically higher WCR and TLC rates (Figure 12). In this case, the risk of TLC was considerable with a rate of 0.3 mm/year. WCR as high as 1.8 mL/(m<sup>2</sup>.s) were predicted at the top of the line, preventing the formation of a stable and protective FeCO<sub>3</sub> layer. Although WCR and TLC rates are related, a large increase in the WCR (case 1 vs. case 2) does not automatically lead to a corresponding large increase in TLC rate, since other parameters, such as the wall temperature, also affect the kinetics of the corrosion

reactions [10]. Anyhow, this confirms, if needs be, the benefits of thermally insulating wet gas pipeline to mitigate TLC.

Case 3, corresponding to the 90° insulation damage, yielded maximum TLC rates of 0.2 mm/year, while the predicted WCR picked at 0.1 mL/(m<sup>2</sup>·s). In this case, the risk of TLC was moderate. Other production conditions (not shown in this study) yielded rates as high as 0.25 mm/year. In addition, the TLC rate calculated at the insulation damage is considerably higher than at the top of the line, as the WCR is also higher.

Case 4, corresponding to the 30° insulation damage, was comparatively less severe. The location of the damage was much closer to the liquid level line and the corresponding drop in wall temperature was consequently less sharp. This led to a lower WCR and consequently a lower TLC rate. Since the predicted TLC rate never (or barely) surpassed 0.1 mm/year, the risk of corrosion in this case was determined as low.

In 2019, an internal inspection of the pipeline was performed using a pig equipped with acoustic resonance technology, able to detect anomalies greater than 0.5 mm in depth. With the insulation damages having occurred in 2016, and the most conservative prediction of TLC rate being 0.2 mm/yr (case 3), the wall thickness loss was expected to be 0.6 mm or less. The inspection detected no corrosion anomalies, which is consistent with the rates predicted in this study.

## CONCLUSIONS

The objective of this work was to estimate the effect of external insulation damage on TLC of two wet gas flowlines. To do so, local conditions affecting TLC were precisely defined and modelled.

This work was performed using a Flow Assurance Software to develop temperature mapping of the entire internal surface of the pipe. TLC predictions were performed using a mechanistic Corrosion Software at the local point of insulation damages.

FEA determined the temperature profile and quantified the WCR for both intact and damaged insulation cases. Subsequent TLC modeling confirmed that the risk of TLC was very low under intact insulation, while a moderate corrosion risk existed at the cold spots corresponding to insulation damages. In this case, mitigation strategies will need to be put in place as TLC rates may be too high to be accommodated by the pipe corrosion allowance.

Overall, the combination of FEA, CFD, water condensation and TLC modelling was successfully used to predict TLC rate for pipe with damaged insulation. This resulted in the optimization of timing for subsequent inspection and repair strategies.

## REFERENCES

1. Nordsveen N., Nestic S., Nyborg R., Stangeland A., "A Mechanistic Model for Carbon Dioxide Corrosion of Mild Steel in the Presence of Protective Iron Carbonate Films - Part 1: Theory and verification", *Corrosion*, 59(5), 443-456, 2003.
2. Nestic S., Nordsveen N., Nyborg R., Stangeland A., "A Mechanistic Model for Carbon Dioxide Corrosion of Mild Steel in the Presence of Protective Iron Carbonate Films - Part 2: A numerical experiment", *Corrosion*, 59(6), 489-497, 2003.
3. Nestic S., Nordsveen N., Nyborg R., Stangeland A., "A Mechanistic Model for Carbon Dioxide Corrosion of Mild Steel in the Presence of Protective Iron Carbonate Films - Part 3: Film growth model", *Corrosion*, 59(7), 616-628, 2003.

4. Z. Zhang, D. Hinkson, M. Singer, H. Wang, S. Nestic, "A Mechanistic Model for Top of the Line Corrosion", *Corrosion*, 63(11), 1051-1062, 2007.
5. U. Kaewpradap, M. Singer, S. Nestic, S. Punpruk, "Comparison of Model Predictions and Field Data – the Case of Top of the Line Corrosion", *Corrosion*, 73(8), 1007-1016, 2017.
6. Thermal Conductivity of Deepwater Offshore Sediments, Newson & Brunning, IJOPE Paper No. TM31, 27-Apr-2004
7. Incropera & de Witt, "Introduction to Heat Transfer", Third Edition, Wiley, 1996
8. Comparison of Soil Models in the Thermodynamic Analysis of a Submarine Pipeline Buried in Seabed Sediments, Magda, W., *Polish Maritime Research* 4 (96), 2017, Vol 24
9. Thermal Conductivity of Deepwater Offshore Sediments, Newson & Brunning, IJOPE Paper No. TM31, 27-Apr-2004
10. Singer, "Study of the Localized Nature of Top of the Line Corrosion in Sweet Environment", *Corrosion* 73(8), 1030-1055, 2017.